Finite Control Set Model Predictive Field-Oriented Control For Three-Phase Induction Motor Drives

DOI : 10.36909/jer.17399

Muhammad Azhar Ghauri, Muhammad Abbas Abbasi*, Muhammad Bilal Shahid, Muhammad Noman, Hafiz Muhammad Ahmad Hakeem

Department of Electronic Engineering, Faculty of Engineering, The Islamia University of Bahawalpur, Pakistan

* Corresponding Author: abbas.abbasi@iub.edu.pk

ABSTRACT

Field-oriented control is one of the well-established vector control strategies for induction motor drives. However, its cascaded structure and requirement of a modulator for constant switching frequency operations makes it complex and computationally expensive. Model predictive control (MPC) is a novel control strategy used for AC motor drives. In this paper, a finite control set model predictive control (FCS-MPC) based field-oriented control (FOC) is presented. The Finite control set model predictive field-oriented control (FCS-MPFOC) utilizes a cost function that quantifies the error between the reference and anticipated current values for all the potential voltage vectors of the voltage source inverter. The voltage vector that generates the lowest value of the cost function is directly implemented on the inverter to produce the drive voltage. The efficiency of the proposed method is authenticated by using a three-phase induction motor, fed via a two-level three-phase voltage source inverter in the MATLAB/Simulink environment under various speeds, load torque, and model parameter mismatch situations. In order to authenticate the performance of the proposed strategy, it is compared with traditional model predictive torque control. Simulation results show that the proposed method performed significantly well in total current harmonic distortion, flux and torque ripples, switching frequency, and parameter variations.

Keywords: Control Drive, Model Predictive Control, Field-Oriented Control, FCS-MPC, MPTC

INTRODUCTION

The induction motor (IM) has become the most popular choice for high-performance industrial applications, electric vehicles, and renewable energy conversion systems (e.g., wind energy). Approximately 90% of the industrial load is shared by the IM because of its simple and resilient design, self-starting characteristics, and requirements for almost little to no maintenance (Zerdali & Demir, 2021)(Abo-Khalil & Sayed, 2021). Thus, a sufficient amount of generated electric power has been utilized by IM around the globe. The growing concerns about the energy crisis and environmental pollution emphasize the importance of an appropriate high-performance drive control strategy for efficient use of energy (Arshad et al., 2019).

Typically, Field-Oriented Control (FOC) and Direct Torque Control (DTC) are the most widely utilized vector control strategies for power electronics and IM motor drives at the industrial level. FOC is a linear control strategy and is implemented with PI controllers and pulse width modulator (PWM). PWM generates firing pulses for the inverter switches in order to generate the drive voltage at a fixed switching frequency while the PI controllers are utilized to regulate the torque and flux error. Although FOC offers a fast steady-state and dynamic response with low current THD and minimum torque and flux ripples, its cascaded structure and utilization of four PI controllers require tuning of various parameters. On the other hand, DTC is a nonlinear control strategy and utilizes hysteresis controllers for the regulation of both electromagnetic torque and flux. It utilizes a predefined switching (LUT) table to select a voltage vector based on the hysteresis controller output in the absence of a PWM modulator. Despite its quick dynamic response, DTC suffers from excessive torque, flux ripples, and increased current distortion at low speeds due to the exclusion of the current loop. Moreover, it operates on a variable switching frequency, which increases the switching losses in the inverter (Martinez-Hernandez et al., 2016)(Favato et al., 2019)(Le-Huy, 1999).

Despite the fact that FOC and DTC are adequate to meet the requirements of the majority of IM drive applications, there is a need to develop the most advanced and sophisticated IM drive control strategy. Fortunately, the advancement in microprocessors and field programmable gate array (FPGA) in recent decades makes it possible to develop advanced control strategies for electrical drives (Wang et al., 2018). Therefore, MPC caught the special attention of researchers for the control of power electronics converters (Jin et al.,

2017)(Abdel-Rahim & Wang, 2020) and electrical drives. In comparison to classical vector control strategies, MPC is viewed as a powerful alternative because of its intuitive concept, quick dynamic response, and ability to handle various nonlinear constraints (Stellato et al., 2016). In MPC, the control decision is implemented by reducing the cost function over a receding prediction horizon in order to produce the desired control response. The cost function is formulated with respect to the control objective by utilizing the control variables, while the future behavior of the system is anticipated by utilizing the system mathematical model. (Tenconi et al., 2018)(Pérez-Guzmán et al., 2020).

The MPC is classified into two main categories: continuous control set MPC (CCS-MPC) and finite control set MPC (FCS-MPC). The CCS-MPC algorithm has been successfully implemented to control the drive of AC machines. However, the algorithm of CCS-MPC is complex and increases computational effort. Furthermore, it necessitates the use of a modulator that increases the complexity of the control system (Wendel et al., 2018)(Wendel et al., 2019)(Borreggine et al., 2019), while, FCS-MPC is a simple control algorithm, requires no modulator, and is extensively employed in controlling the AC machines. (Gonçalves et al., 2019)

Predictive torque control (PTC) was the first control strategy presented with FCS-MPC for IM drives, while predictive current control (PCC) was the first control strategy implemented with FCS-MPC to control the 2L-VSI with RL load. Both these FCS-MPC strategies utilize the inverter model in the cost function, and an optimal output voltage vector is directly applied to the inverter without any modulator. The cost function of PTC minimizes the error of electromagnetic torque and flux between their absolute predicted and reference values. Moreover, as the cost function of PTC includes the terms of non-identical units, a weighting factor is utilized to give the relative importance to each term. The weighting factor depends upon torque and flux values and needs to be calculated earlier before being given to the cost function. Whereas, the cost function of PCC includes the predicted and reference values of stator current in the αβ frame and minimizes the error between them. The PCC control algorithm is simple, and the cost function includes current terms only; therefore, no weighting factor is required (Nemec et al., 2007)(Jos Rodriguez et al., 2007). In the literature, the PCC demonstrates higher efficiency than the PTC and is rarely adopted to control the IM drive. (Wang et al., 2017). However, due to the absence of a modulator, both PCC and PTC operates at a variable switching frequency, which not only increases the switching losses in the inverter but also affects the systems steady-state performance.

The main goals of this paper are to control the switching frequency of FCS-MPC in acceptable range and to eradicate the structural and computational complexity of FOC to enhance the stability and performance of the drive control system. In order to achieve these goals, the authors merge the FOC with FCS-MPC in this paper. The simulation results show the effectiveness of the proposed control strategy at different speeds under load and no-load conditions in terms of current THD, flux, torque quality, switching frequency, and parameter mismatch situations. Moreover, the performance authentication of the proposed strategy has been done by comparing its result with traditional model predictive torque control (MPTC)- the proposed strategy demonstrates the superiority over MPTC. The rest of the paper will describe the mathematical models of IM and 2L-3ω voltage source inverters, the FCS-MPFOC methodology, simulation results, and conclusion.

MATHEMATICAL MODEL OF IM

The following mathematical equations describe the mathematical model of the three-phase squirrel cage induction motor in $\boldsymbol{\alpha\beta}$ reference frame:(Jose Rodriguez & Cortes, 2012)

$$\boldsymbol{v_s} = R_s\boldsymbol{i_s} + \frac{d\boldsymbol{\psi_s}}{dt} \quad (1)$$

$$0 = R_r\boldsymbol{i_r} + \frac{d\psi_r}{dt} - j\omega_r\,\boldsymbol{\psi_r} \quad (2)$$

$$\boldsymbol{\psi_s} = L_s\boldsymbol{i_s} + L_m\boldsymbol{i_r} \quad (3)$$

$$\boldsymbol{\psi_r} = L_r\boldsymbol{i_r} + L_m\boldsymbol{i_s} \quad (4)$$

$$T_e = 1.5.p.I_m[\overline{\boldsymbol{\psi_s}}\boldsymbol{i_s}\,] = -1.5.p.I_m[\overline{\boldsymbol{\psi}}_{\boldsymbol{r}}\boldsymbol{i_r}] \quad (5)$$

$$J\frac{d\omega_m}{dt} = T_e - T_l \quad (6)$$

Where; $\boldsymbol{v_s}$, $\boldsymbol{i_s}$, $\boldsymbol{\psi_s}$ And represent stator voltage, current, and flux vector. While $\boldsymbol{\psi_r}$, $\boldsymbol{i_r}$ represents the rotor flux and rotor current vector. $\boldsymbol{T_e}$, $\boldsymbol{T_l}$, $\boldsymbol{\omega_r}$ and $\boldsymbol{\omega_m}$ represents the electromagnetic torque, load torque, rotor electrical, and mechanical speed, respectively. $\boldsymbol{R_s}, \boldsymbol{R_r}$ are the stator and rotor side resistance, where $\boldsymbol{L_s}$, $\boldsymbol{L_r}$ are the stator and rotor inductance; $\boldsymbol{L_m}$ is the mutual inductance. The $\boldsymbol{p}$ is the number of pole pairs and $\boldsymbol{J}$ represents the moment of inertia. $\boldsymbol{\psi_s}, \boldsymbol{\psi_r}$ shows the complex conjugate of rotor and stator flux vector and $\boldsymbol{I_m}$ denotes the imaginary part of the complex vector.

MATHEMATICAL MODEL OF 3$\boldsymbol{\varphi}$ VOLTAGE SOURCE INVERTER

The two-level 3φ voltage source (2L-VSI) inverter is presented in Figure 1a. The 2L-VSI is made up of six semiconductor switches and placed on three legs so that each leg has two

switches. The switches operate in such a way that only one switch from each leg conducts at a time. The switching states can be represented in a vectorial form as:

$$S = \frac{2}{3}(S_a + \boldsymbol{K}S_b + \boldsymbol{K^2}S_c) \qquad (7)$$

Where; $\boldsymbol{K} = e^{j(2\pi/3)}$

The voltage utilized to drive the IM can be represented as:

$$\boldsymbol{v} = \boldsymbol{S}.V_{dc} \qquad (8)$$

The 2L-VSI has eight switching vectors (0 to 7), of which six (1 to 6) are active vectors, and two (0 and 7) are inactive or zero vectors. The zero vectors do not produce any output voltage. However, they are utilized to minimize the switching losses of the inverter. The Figure 1b depicts the 2L-VSI vectors in αβ reference frame (Kazmierkowski, 2012).

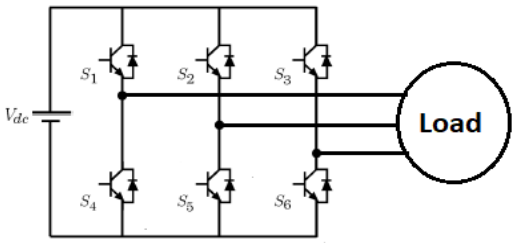

FIGURE 1a- 2L-VSI

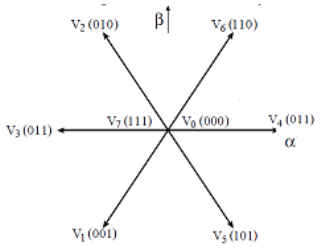

FIGURE 1b- 2L-VSI output voltage vector's

FINITE CONTROL SET MODEL PREDICTIVE FIELD-ORIENTED CONTROL

Figure 2 illustrates the finite control set model predictive field-oriented control (FCS-MPFOC) for induction motor drive. It utilizes the rotor field orientation, similar to the traditional FOC. Unlike FOC, only one PI controller is used to regulate the rotor speed error, and the PWM block is also eliminated, which makes the control scheme simpler and less computational. In the current simulation study, the field weakening was not investigated. The workflow of FCS-MPFOC in detail is described below.

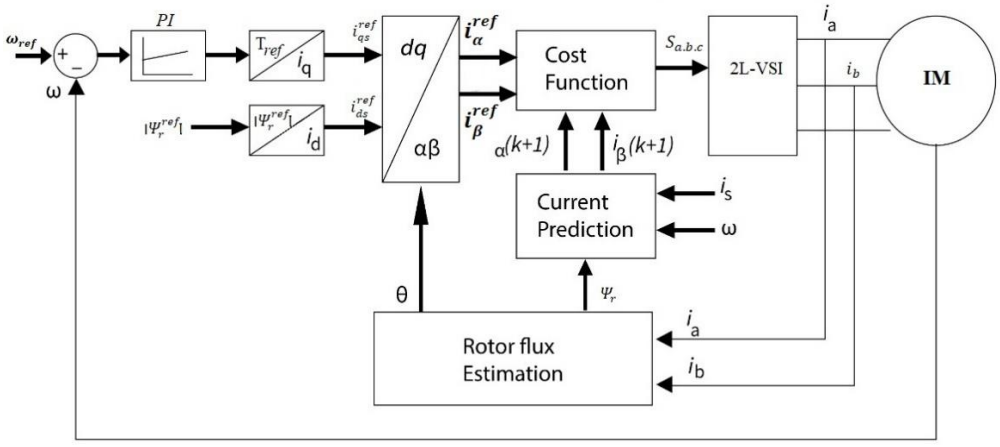

Figure 2. FCS-MPFOC for three-phase IM

MEASUREMENT

The rotor speed is obtained via a sensor placed on the IM motor shaft. The obtained rotor speed and stator current in $\alpha\beta$ reference frame are provided as feedback. The reference torque (T_{ref}) is obtained by regulating the actual and reference speed errors by the PI controller while the reference rotor flux remains constant. The following equations are utilized to obtain the torque and flux generating components of stator current in the rotor flux reference frame.

$$\boldsymbol{i_{ds}^{ref}} = \frac{|\boldsymbol{\psi_r^{ref}}|}{L_m} \tag{9}$$

$$\boldsymbol{i_{qs}^{ref}} = (0.66).\frac{L_r}{L_m}.\frac{T_{ref}}{|\boldsymbol{\psi_r^{ref}}|} \tag{10}$$

ROTOR FLUX ESTIMATION

The rotor flux estimation and position of the rotor flux are important for FCS-MPFOC. The θ is used in reference current transformation for dq to $\alpha\beta$, while the estimated rotor flux utilizes in the cost function of the predictive controller for next-step current predications. The rotor flux can be computed as:

$$\boldsymbol{\psi_r} = L_r\boldsymbol{i_r} + L_m\boldsymbol{i_s} \tag{11}$$

The decomposed rotor flux in αβ reference frame can be obtained by following equations

$$\boldsymbol{\psi_{r\alpha}} = \frac{L_r}{L_m}(\boldsymbol{\psi_{s\alpha}} - \delta L_s\boldsymbol{i_{s\alpha}}) \tag{12}$$

$$\boldsymbol{\psi_{r\beta}} = \frac{L_r}{L_m}\left(\boldsymbol{\psi_{s\beta}} - \delta L_s\boldsymbol{i_{s\beta}}\right) \tag{13}$$

The rotor flux magnitude is computed as

$$|\boldsymbol{\psi_r}| = \sqrt{\boldsymbol{\psi_{r\alpha}}^2 + \boldsymbol{\psi_{r\beta}}^2} \tag{14}$$

The angle of rotor flux position $\theta\ is$

$$\theta = \tan^{-1}\left(\frac{\boldsymbol{\psi_{r\alpha}}}{\boldsymbol{\psi_{r\beta}}}\right) \tag{15}$$

CURRENT PREDICTION

The stator current is essentially predicted for the all-potential voltage vectors of the inverter, and these predictions are evaluated by the cost function. The stator current of IM can be represented as:

$$\boldsymbol{i_s} = -\frac{1}{R_\sigma}\{[L_\sigma.\frac{\boldsymbol{di_s}}{\boldsymbol{dt}} - k_r.\left[\frac{1}{T_r} - j.\omega\right].[\Psi_r] - v_s] \tag{16}$$

Where; $k_r = {}^{L_m}/_{L_r}$, $L_\sigma = \sigma . L_s$, and $R_\sigma = R_s + k_r^2 . R_r$

The 1st order forward Euler discretization method is utilized to predict the stator current value for the next time step's with T_s. Where, T_s is the systems sampling time

$$\boldsymbol{i_s}(k+1) = \frac{\tau_\sigma}{\tau_\sigma + T_s} . \boldsymbol{i_s}(k) + \frac{T_s}{L_\sigma(\tau_\sigma + T_s)} . \boldsymbol{v_s}(k) + \frac{k_r T_s}{\tau_r L_\sigma(\tau_\sigma + T_s)} . (1\text{-j}.\frac{1}{L_\sigma} . \omega(k)) . \psi_r(k) \qquad (17)$$

where; $L_\sigma = \sigma . L_s$ and $\tau_\sigma = \frac{L_\sigma}{R_\sigma}$.

OPTIMIZATION

In FCS-MPFOC, the optimization process is done through the evaluation of the cost function. It evaluates the value of the cost function for all potential VV's of 2L-VSI represented in Figure 2. Since the 2L-VSI has eight switching states with seven voltage vectors, thus, the value of the cost function is assessed seven times. The VV (voltage vector) that generates the lowest value of the cost function is elected as the optimized VV and is directly applied to VSI in the next time period. The cost function of FCS-MPFOC is

$$g_i = \sum_h^N \Big\{ \mid i_\alpha^{ref} - i_\alpha(k+h)_i \mid + \mid i_\beta^{ref} - i_\beta(k+h)_i \mid + \lambda_w . \mid F_{sw}(k+1) - F_{sw}(k) \mid + I_m(k+h)_i \Big\} \qquad (18)$$

Where, g_i is the value of the cost function. N represents the prediction horizon, while h is the simulation index. For time delay compensation, N=h=2 is considered. The i_α^{ref}, i_β^{ref} and $i_\alpha(k+h)$, $i_\beta(k+h)$ are the decomposed components of stator current in the αβ reference frame. The absolute error is taken between the predicted and reference value to reduce the computational complexity. The next terms in the cost function are the switching frequency control term and the. 'λ_w' is weighting factor which can be tuned to give the relevant importance to this term. The term I_m is the current limiting term and is used to protect the motor from an over current situation. The I_m can be represented as:

$$I_m = \begin{cases} 0 & if \quad \mid i(k+h) \mid \leq \mid I_{max} \mid \\ \gamma \gg 0 & if \quad i(k+h) \mid > \mid I_{max} \mid \end{cases} \qquad (19)$$

where,

$$\mid i(k+h) \mid = \sqrt{\mid {i_\alpha}^2 - i_\alpha(k+h)^2 + {i_\beta}^2 - i_\beta(k+h) \mid} \qquad (20)$$

SIMULATION RESULTS

Simulation results are presented in this section. In order to authenticate the performance of FCS-MPFOC, it is compared with conventional MPTC by using similar test bench and criteria in the MATLAB/Simulink environment. The Simulation parameters are presented in Table 1. The controller sampling time and frequency are 40μs and 25 KHz, respectively.

The efficiency of the FCS-MPFOC drive strategy is mainly determined by stator current THD, torque, flux ripples, switching frequency and model parameter variation environment. The performance of the controller is validated by performing speed reversal, load, and no-load tests at full rated and low speed (30% of the rated speed) and in model parameter mismatch situations.

Table.1. Simulation setup parameters

Parameters	Notation	Values	Parameters	Notation	Values
DC-Link Voltage	V_{dc}	240V	Stator Resistance	R_s	3 Ω
Rotor Resistance	R_r	4.1 Ω	Stator Inductance	L_s	0.3419 H
Rotor Inductance	L_r	0.3513 H	Pole Pair	p	1
Nominal Torque	T_{nom}	5 Nm	Rated Speed	ω	65 rad/sec
Moment of Inertia	J	0.0117 K_g/m^2	Magnetizing Inductance	L_m	0.324 H
Rotor reference flux	ψ_r^{ref}	0.75 Wb			

Figure.3 illustrates the performance of FCS-MPFOC and MPTC under speed reversal operation. In this test, IM is suddenly reversed from its full speed of 65 rad/s to a speed of -65 rad/s. FCS-MPFOC showed higher performance than traditional MPTC in this test. It is evident from the speed response that FCS-MPFOC completed the transition process in just 0.3s (from $t = 0.2s$ to $t = 0.5s$) while MPTC took 0.5s (from $t = 0.15s$ to $t = 0.65s$) to achieve the transition. It could be seen clearly that torque in both strategies reaches its maximum value of 5Nm when the motor is deaccelerated from its peak speed. Despite the fact that torque and stator flux maintain their smoothness when the motor is controlled by FCS-MPFOC, a slight increase in stator flux is noticed during the transition time. This is because the applied predicted VV and the voltage vector that produces more torque caused the fluctuations in stator flux. Whereas, this is not the case in MPTC stator flux remained at its nominated value. However, the amount of torque and flux ripples is quite higher in MPTC due to the inclusion of a weighting factor in the cost function. Moreover, it introduced more distortion in the inverter's output voltage, while in FCS-MPFOC, the inverter voltage followed almost the sinusoidal waveform without having any noticeable distortion with a constant amplitude of 160v. In terms of current response, FCS-MPFOC showed higher stability and smoothness than MPTC because of its cost function, which regulates the current error only.

The comparison of FCS-MPFOC and MPTC under full load conditions is demonstrated in Figure 4. To evaluate the performance of both strategies, a rated load of 5Nm is employed when the motor is running at its full speed. It can be seen clearly that motor speed in FCS-MPFOC and MPTC has been dropped to 5rad/sec and 3rad/sec, respectively. In FCS-MPFOC, the magnitude of stator flux increased from its true value while it remained unchanged in MPTC. An increase in stator current is also observed in both strategies, because the motor draws more power to balance the load torque under the load condition. However, the THD of stator current in MPTC, with 3.8%, is slightly higher than the 3.6% of FCS-MPFOC. The FCS-MPFOC experienced low torque and flux ripples with 0.38Nm and 0.02Wb, respectively. Whereas, the torque and flux ripples were slightly higher in MPTC, with 0.43Nm and 0.03Wb for each. Similarly, the average switching frequency for MPTC was noticed at 7.05KHz, which is considerably higher than the 6.06KHz of FCS-MPFOC. Furthermore, the inverter voltage response of MPTC improved in comparison to its previous one, while it remained at the same level without any considerable changes for FCS-MPFOC. The steady state performance of FCS-MPFOC and MPTC has been depicted in Figure 5. Both strategies showed excellent steady-state performance. In terms of flux ripples, only 0.008Wb has been observed for the former one, while 0.025 was noticed for the latter one. Similar performance was observed for torque ripples-MPTC witnessed 0.06Nm while 0.04Nm was observed for FCS-MPFOC. Moreover, the efficiency of FCS-MPFOC and MPTC showed satisfactory performance for stator current. The THD of the current $\boldsymbol{i_\alpha}$ for MPTC and FCS-MPFOC was observed at 3.85% and 3.68%, respectively, which is slightly higher than under load operation. This happened due to the lower average switching frequency, which was recorded at 4.5KHz for MPTC and 3.9KHz for FCS-MPFOC. Furthermore, MPTC introduced more distortion in the voltage waveform; however, it remained almost sinusoidal for FCS-MPFOC.

FCS-MPFOC and MPTC performance were also investigated at low speeds under full load conditions. The same simulation parameters are utilized as were used at rated speed except for the IM speed, which was reduced to 30% of its rated speed (20rad/s). The performance comparison of both strategies has been illustrated in figure 6. It is observed that the speed characteristic of the FCS-MPFOC has been improved and only reduced by 3rad/s, while in MPTC a 4rad/s reduction was noticed when the motor was dragging the load of 5Nm. However, the inverter's voltage waveform has improved and has become more sinusoidal for MPTC. Both strategies showed similar characteristics as those shown under full load operation in the rest of the performance evaluation criteria. The average switching

frequency, on the other hand, was made better and went down to 4.52KHz for FCS-MPFOC and 5.68KHz for MPTC.

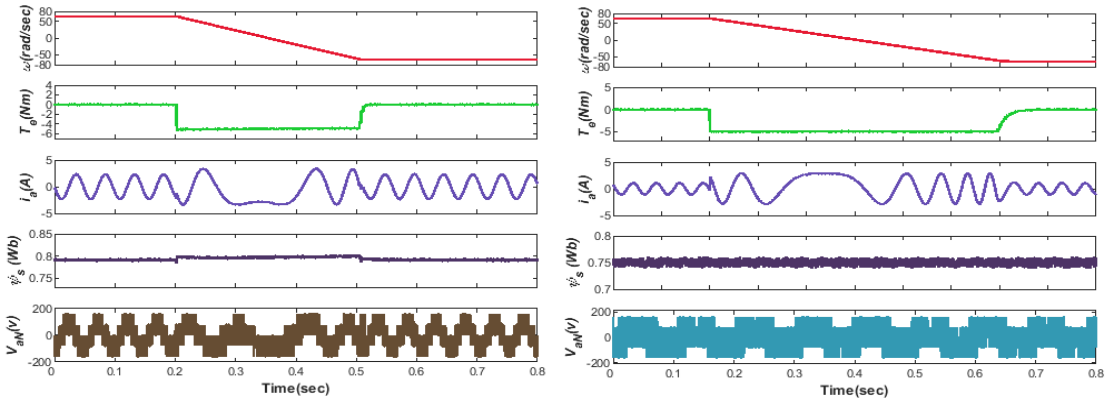

(a) **(b)**

Figure 3. Speed reversal behavior at rated speed **a)** FCS-MPFOC **b)** MPTC

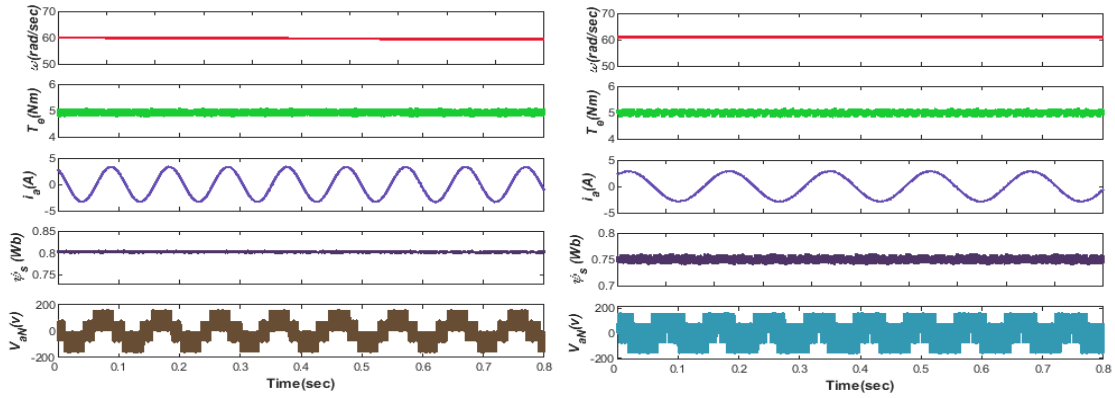

(a) **(b)**

Figure 4. Full-load perfromance authentication at rated speed **a)** FCS-MPFOC **b)** MPTC

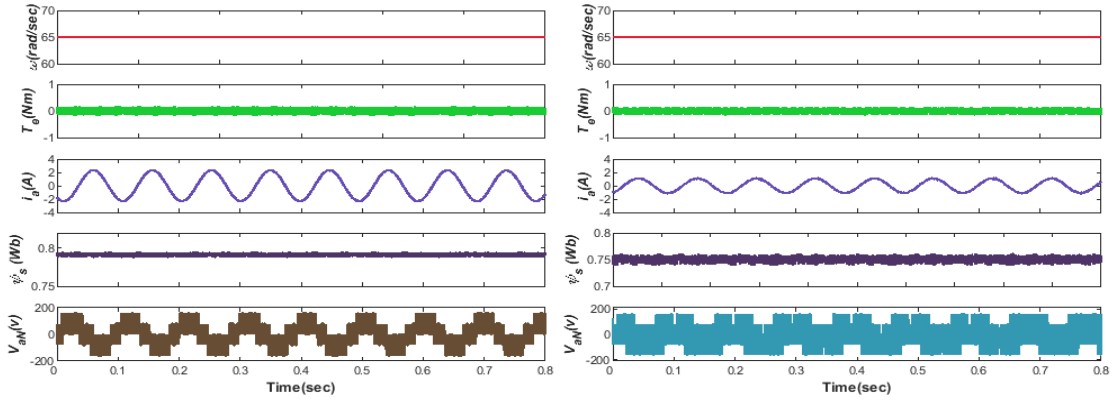

(a) **(b)**

Figure 5. Steady-state analysis at rated speed **a)** FCS-MPFOC **b)** MPTC

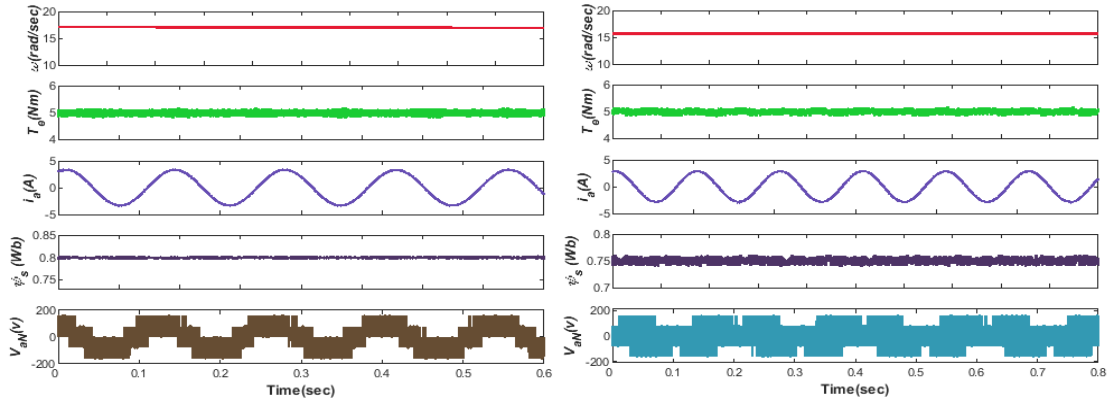

(a) **(b)**

Figure 6. Performance validation at low speed **a)** FCS-MPFOC **b)** MPTC

FCS-MPFOC ROBUSTNESS ANALYSIS AGAINST PARAMETERS DEVIATION

FCS-MPFOC is a nonlinear control scheme that utilizes the dynamic model of the induction motor for electing the optimal operation. The IM model parameters can vary under certain operating conditions. It is essential to analyze how FCS-MPFOC will react if the parameters of IM change. Therefore, the responsiveness of the FCS-MPFOC against the R_s, L_m variations are also investigated in this research paper.

The induction motor operates continuously under loaded conditions in the industries. Due to the continuous operation, the motor windings get heated, which results in a change in stator resistance value. Thus, the FCS-MPFOC system stability against stator resistance mismatch is essential to investigate. The FCS-MPFOC performance in the case of R_s deviation under various operating conditions is investigated in this test and compared with MPTC to authenticate its performance under the same scenarios. Figure 7 illustrates the simulation results of both strategies in case of R_S variation under zero load at rated speed. The results showed that the FCS-MPFOC was heading towards instability as the value of R_s increased by 30% of its initial value. The stator flux lost its smoothness, and torques became more distorted. In spite of FCS-MPC, MPTC showed great robustness and hardly affected in terms of torque and flux ripples, however, the distortion in stator current has been increased as compared to FCS-MPFOC. Moreover, MPTC introduced more distortion in the inverter's output voltage waveform while a few spikes were also noticed in the FCS-MPFOC inverter's output voltage waveform.

Figure 8 shows the performance of FCS-MPFOC and MPTC in the case of R_s variation under full load of nominal torque value at rated speed. It is evident that the FCS-MPOC system is more sensitive than MPTC when the value of R_s increased to 15% of its initial

value under load conditions. The stator flux and torque have been distorted and became sinusoidal in FCS-MPFOC, while in they are hardly affected in MPTC. However, more distortion was noticed in the current and output voltage waveforms than in FCS-MPFOC.

The performance comparison of FCS-MPFOC and MPTC is also conducted in case of L_m deviation. As the stator flux of an induction motor is derived from the ratio of live measured current and L_m. Therefore, the L_m variation induces a high estimation inaccuracy in flux estimation, which leads to system instability. So, it is essential to authenticate the performance of FCS-MPFOC under L_m variation. Figure 9 represents the L_m mismatch behavior of FCS-MPFOC and MPTC at nominated speed without having any load on the IM shaft. The value of L_m for FCS-MPFOC was increased to 20%, while it was decreased to 20% for MPTC. In the case of FCS-MPFOC the stator flux was reduced with the increase of L_m, while it was observed constant at its nominal value in MPTC. However, the torque response of MPTC has been distorted while it remained smooth in FCS-MPFOC. Moreover, the inverter's output voltage waveform was improved significantly and followed almost sinusoidal.

Figure.10 compares the performance of both strategies in the case of L_m variation under full load at rated speed. The variation in the value of L_m has remained the same as in previous test. It can be observed clearly that the torque and stator flux of MPTC were distorted while they remained less noisy for FCS-MPFOC. Similarly, the distortion in the stator has increased to a significant value in MPTC as compared to FCS-MPFOC, which showed a more stable and smooth current response.

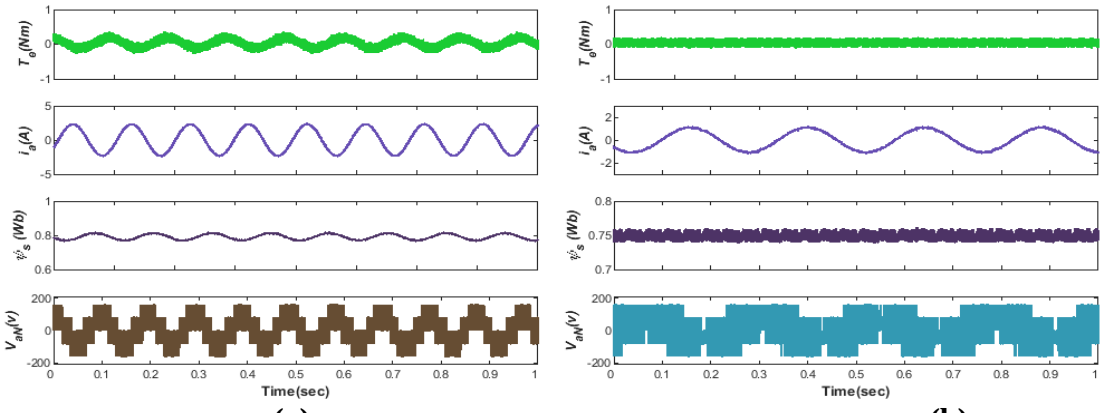

(a) **(b)**

Figure 7. R_s sensitivity analysis at zero-load under rated speed **a)** FCS-MPFOC **b)** MPTC

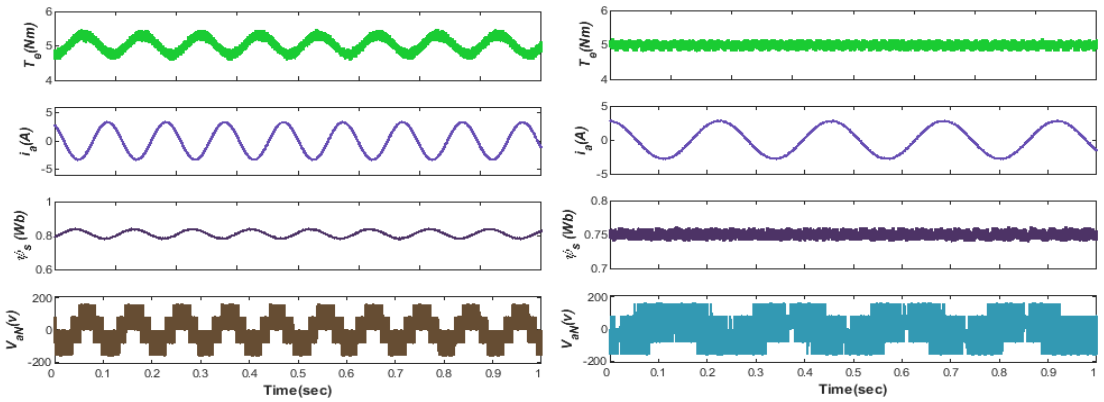

(a) **(b)**

Figure 8. R_s variation validation at load under full speed **a)** FCS-MPFOC **b)** MPTC

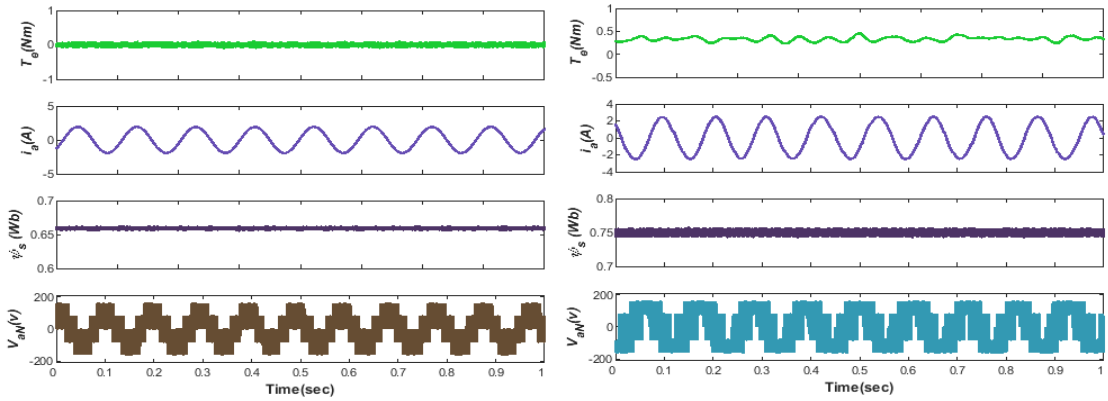

(a) **(b)**

Figure 9. L_m mismatch analysis at no-load rated speed **a)** FCS-MPFOC **b)** MPTC

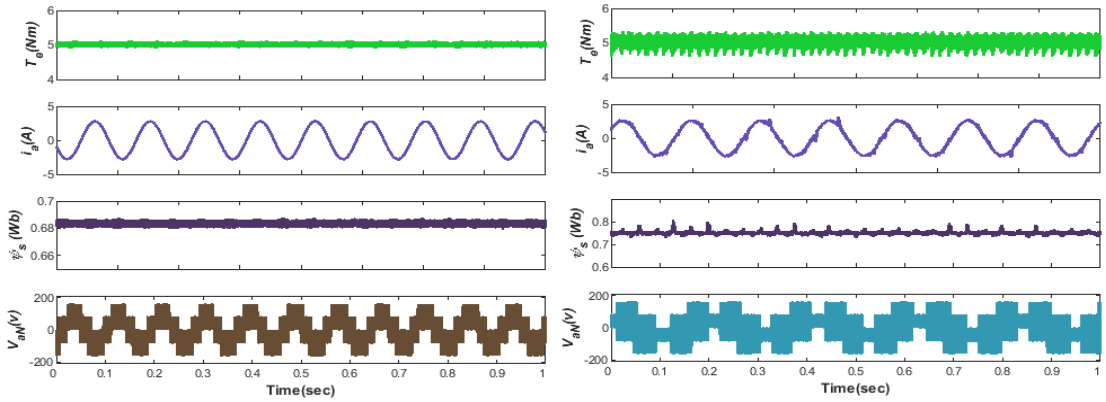

(a) **(b)**

Figure 10. L_m mismatch analysis at load under rated speed **a)** FCS-MPFOC **b)** MPTC

CONCLUSION

A finite control set model predictive control (FCS-MPC) is merged with field-oriented control to enhance the steady-state and transient response and to reduce the structural and computational complexity of FOC for induction motor drives. FCS-MPFOC successfully reduces the complexity of the drive control system and shows a fast-dynamic response due

to the omission of an inner current loop and modulator. To authenticate the effectiveness of the FCS-MPFOC, it was compared to traditional MPTC in terms of stator current THD, flux, torque ripples, and switching frequency. The simulation results authenticate FCS-MPFOC's superiority over MPTC. The flux and current remain smooth at almost all speeds of operation, and the system's switching frequency remains significantly low. Moreover, computational time in FCS-MPFOC is smaller than MPTC, which reduces the required computational power of the microprocessor. The robustness of FCS-MPFOC against parameter variation is also authenticated under the various drive conditions. The controller performs more robustly at high speed. The simulation study reveals that the controller has good robustness against R_s variation at high speed. However, the R_s sensitivity of the controller increased at low-speed operation. FCS-MPFOC more sensitive to L_m deviation at both low and high-speeds. This research will be extended by using a parameter observer in order to deal with parameter sensitivity in the future.

REFERENCES

Abdel-Rahim, O., & Wang, H. 2020. A new high gain DC-DC converter with model-predictive-control based MPPT technique for photovoltaic systems. *CPSS Transactions on Power Electronics and Applications*, *5*(2), 191–200.

Abo-Khalil, A. G., & Sayed, K. 2021. WIND TURBINE SIMULATION AND CONTROL USING SQUIRREL-CAGE INDUCTION GENERATOR FOR DFIG WIND ENERGY CONVERSION SYSTEMS. *Sohag Engineering Journal*, *1*(1), 1–15.

Arshad, M. H., Abido, M. A., Salem, A., & Elsayed, A. H. 2019. Weighting factors optimization of model predictive torque control of induction motor using NSGA-II with TOPSIS decision making. *IEEE Access*, *7*, 177595–177606.

Borreggine, S., Monopoli, V. G., Rizzello, G., Naso, D., Cupertino, F., & Consoletti, R. 2019. A review on model predictive control and its applications in power electronics. *2019 AEIT International Conference of Electrical and Electronic Technologies for Automotive (AEIT AUTOMOTIVE)*, 1–6.

Favato, A., Carlet, P. G., Toso, F., & Bolognani, S. 2019. A novel formulation of continuous control set mpc for induction motor drives. *2019 IEEE International Electric Machines & Drives Conference (IEMDC)*, 2196–2202.

Gonçalves, P., Cruz, S., & Mendes, A. 2019. Finite control set model predictive control of six-phase asymmetrical machines—An overview. *Energies*, *12*(24), 4693.

Jin, N., Hu, S., Gan, C., & Ling, Z. 2017. Finite states model predictive control for fault-tolerant operation of a three-phase bidirectional AC/DC converter under unbalanced grid voltages. *IEEE Transactions on Industrial Electronics*, *65*(1), 819–829.

Kazmierkowski, M. P. 2012. High Performance Control of ac Drives with MATLAB/Simulink Models [Book News]. *IEEE Industrial Electronics Magazine*, *6*(4), 68–69.

Le-Huy, H. 1999. Comparison of field-oriented control and direct torque control for induction motor drives. *Conference Record of the 1999 IEEE Industry Applications Conference. Thirty-Forth IAS Annual Meeting (Cat. No. 99CH36370)*, *2*, 1245–1252.

Martinez-Hernandez, M. A., Gutierrez-Villalobos, J. M., Malagon-Soldara, S. M., Mendoza-Mondragon, F., & Rodriguez-Resendiz, J. 2016. A speed performance comparative of field oriented control and scalar control for induction motors. *2016 IEEE Conference on Mechatronics, Adaptive and Intelligent Systems (MAIS)*, 1–7.

Nemec, M., Nedeljkovic, D., & Ambrozic, V. 2007. Predictive torque control of induction machines using immediate flux control. *IEEE Transactions on Industrial Electronics*, *54*(4), 2009–2017.

Pérez-Guzmán, R. E., Rivera, M., & Wheeler, P. W. 2020. Recent advances of predictive control in power converters. *2020 IEEE International Conference on Industrial Technology (ICIT)*, 1100–1105.

Rodriguez, Jos, Pontt, J., Silva, C. A., Correa, P., Lezana, P., Cortés, P., & Ammann, U. 2007. Predictive current control of a voltage source inverter. *IEEE Transactions on Industrial Electronics*, *54*(1), 495–503.

Rodriguez, Jose, & Cortes, P. 2012. *Predictive control of power converters and electrical drives* (Vol. 40). John Wiley & Sons.

Stellato, B., Geyer, T., & Goulart, P. J. 2016. High-speed finite control set model predictive control for power electronics. *IEEE Transactions on Power Electronics*, *32*(5), 4007–4020.

Tenconi, A., Rubino, S., & Bojoi, R. 2018. Model predictive control for multiphase motor drives–a technology status review. *2018 International Power Electronics Conference (IPEC-Niigata 2018-ECCE Asia)*, 732–739.

Wang, F., Mei, X., Tao, P., Kennel, R., & Rodriguez, J. 2017. Predictive field-oriented control for electric drives. *Chinese Journal of Electrical Engineering*, *3*(1), 73–78.

Wang, F., Zhang, Z., Mei, X., Rodríguez, J., & Kennel, R. 2018. Advanced control strategies of induction machine: Field oriented control, direct torque control and model predictive control. *Energies*, *11*(1), 120.

Wendel, S., Haucke-Korber, B., Dietz, A., & Kennel, R. 2018. Cascaded continuous and finite model predictive speed control for electrical drives. *2018 20th European Conference on Power Electronics and Applications (EPE'18 ECCE Europe)*, P-1.

Wendel, S., Haucke-Korber, B., Dietz, A., & Kennel, R. 2019. Experimental Evaluation of Cascaded Continuous and Finite Set Model Predictive Speed Control for Electrical Drives. *2019 21st European Conference on Power Electronics and Applications (EPE'19 ECCE Europe)*, P-1.

Zerdali, E., & Demir, R. 2021. Speed-sensorless predictive torque controlled induction motor drive with feed-forward control of load torque for electric vehicle applications. *Turkish Journal of Electrical Engineering & Computer Sciences*, *29*(1), 223–240.